Making Cytometry of Reaction Rate Constant (CRRC) Applicable to Motile Cells

Robel Yosief,[1#] Giammarco Nebbioso,[1#] Vasilij Koshkin,[1] Yumin Qiu,[2] Chun Peng,[2] Vadim Elisseev,[3] and Sergey N. Krylov*[1]

[1] Department of Chemistry and Centre for Research on Biomolecular Interactions, York University, Toronto, Ontario M3J 1P3, Canada
[2] Department of Biology and Centre for Research on Biomolecular Interactions, York University, Toronto, Ontario M3J 1P3, Canada
[3] IBM Research Europe, The Hartree Centre, Daresbury Laboratory, Warrington WA4 2AD, UK and Wrexham Glyndwr University, Mold Rd, Wrexham LL11 2AW, UK

[#]These authors contributed equally

*Corresponding author's email: skrylov@yorku.ca

ABSTRACT: Cytometry of Reaction Rate Constant (CRRC) is a method for studying heterogeneity of cell populations with regards to activity of cellular reactions. It is based on time-lapse fluorescence microscopy which facilitates following reaction kinetics in individual cells. The current CRRC workflow utilizes a single fluorescence image to manually identify cell contours; these contours are then used to determine fluorescence intensity of individual cells in the entire time-stack of images. This workflow can only be used reliably if the cells maintain their positions during the time-lapse measurements; if the cells move, the results of a CRRC experiment will be inaccurate. The requirement of invariant cell positions during a prolonged imaging is impossible to satisfy for motile cells. Here we report on developing an advanced workflow that makes CRRC applicable to motile cells. The new workflow combines fluorescence microscopy with brightfield (BF) microscopy and utilizes automated processing and analysis of images. A BF image is taken right after every fluorescence image and used to determine cell contours. The contours are tracked through the time-stack of BF images to account for cell movement. A set of contours, which is unique for every image, is then used to determine fluorescence intensity of cells in the associated fluorescent image. Finally, time dependencies of intracellular fluorescence intensities are used to determine the rate constant and plot a kinetic histogram "number of cells *vs* rate constant". The robustness of the new workflow to cell movement was confirmed experimentally by conducting a CRRC study of cross-membrane transport in motile cells. The new workflow makes CRRC applicable to a wide range of cell types and eliminates the influence of cell motility on the accuracy of results.

Cancerous tissues are typically very heterogeneous; a single tumor may be composed of several distinct cell populations, for example, a population of bulk tumor cells and a population of tumor-initiating cells.[1, 2] Quantitative characteristics of tumor composition, e.g., the size of the population of tumor-initiating cells, define its carcinogenic features, e.g., resistance to chemotherapy.[3, 4] Fundamentally, tumor heterogeneity is caused by differences in molecular reactions between the cells. If a reaction is associated with tumor heterogeneity, it can serve as a basis for characterizing the heterogeneity.[5]

Cytometry is a general approach to study tumor heterogeneity via measuring fluorescence at the single-cell level. Cytometry of Reaction Rate Constant (CRRC) is a cytometry technique that follows reaction kinetics at the single-cell level and presents the results as a kinetic histogram "number of cells *vs.* rate constant".[6-11] Rate constants are the most robust parameters to characterize chemical reactions, and, accordingly, CRRC can support robust and accurate characterization of reaction-based cell-population heterogeneity.[12] CRRC may be potentially suitable for the development of reliable cancer biomarkers built upon such heterogeneity.[13]

CRRC is based on time-lapse fluorescence microscopy (Figure 1). Conceptually, a fluorescent or fluorogenic substrate that is involved in the reaction of interest is loaded into the cells. Fluorescent images of a few hundred cells are taken progressively to monitor the change in intracellular fluorescence intensity. The images are processed to obtain a kinetic trace "fluorescence intensity *vs.* time" for each cell and a value of the rate constant is determined from such trace for each cell. Finally, the data are presented as a kinetic histogram: "number of cells *vs.* rate constant".

The current CRRC workflow includes only confocal fluorescence microscopy and utilizes a single fluorescence image to manually identify cell contours. The cell contours identified from this single image are used to determine fluorescence intensity of individual cells in each other image of the large time-stack of images. This workflow assumes that each cell retains its position in the image throughout the entire course of time-lapse measurements. Such an assumption is impossible to satisfy for motile cells which move significantly during the time-lapse measurements. If the cells move, the results of a CRRC experiment will be inaccurate because cell contours used to determine cell fluorescence will not correspond to gradually changing positions of the cells. Thus, making CRRC robust to cell movement requires a new workflow that identifies cell contours for each image and tracks cell contours through the time-stack of images. Here we report on the successful development of such a workflow.

Conceptually, the new CRRC workflow combines two types of

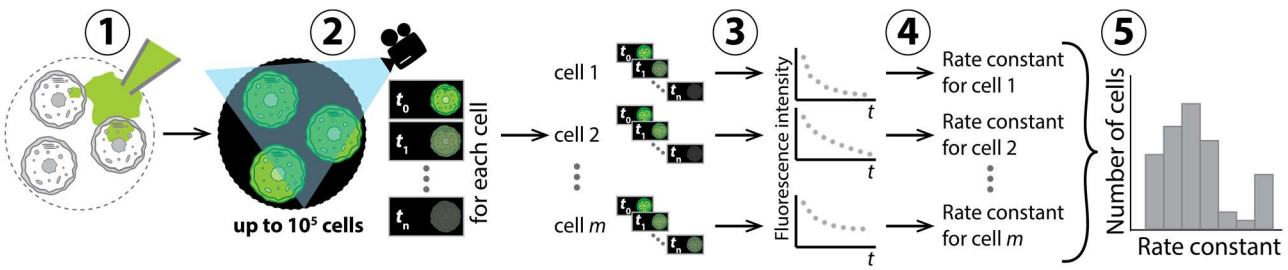

Figure 1. Schematic depiction of Cytometry of Reaction Rate Constant. See text for details.

optical microscopy: (*i*) transmitted light microscopy for cell-contour identification and cell tracking through the time-stack of images and (*ii*) fluorescence microscopy for monitoring substrate conversion into the product during the time-lapse imaging. Imaging is done in an automated fashion with a transmitted light image taken immediately after every fluorescence image. Time-correlated stacks of fluorescence and transmitted-light images are processed and analyzed automatically to produce kinetic traces "fluorescence intensity *vs* time" which are invariant to cell displacement.

The proof of concept included four major steps. First, we compared three modes of transmitted light microscopy — bright field (BF), phase contrast (PC), and differential interference contrast (DIC) — and concluded that BF is the most reliable mode for cell-contour identification. Second, we proved that cell displacement between the adjacent fluorescent and BF images is negligible even for highly-motile cells; hence, cell contours determined from BF images are applicable to fluorescence images. Third, we proved that the new workflow is not affected by the difference in focal plane positions between BF and fluorescence imaging. Finally, we conducted a comparative study of the original and new workflows in CRRC of cross-membrane transport in motile cells. The results clearly demonstrated that the original workflow was not robust to cell motility while the new workflow was.

MATERIALS AND METHODS

Cell Culture. Ovarian cancer cells TOV-112D were purchased from ATCC and maintained in MCDB 105/Medium 199 (Sigma-Aldrich, St. Louis, MO, USA, Cat. No. of MCDB 105: M6395, Cat. No. of Medium 199: M5017) supplemented with 10% fetal bovine serum (Gibco, Grand Island, NY, USA, Cat. No: 12483-020). Cells were cultured in 60 mm plates (Sarstedt AG&Co, Numbrecht, Germany, Cat. No: 83.3901) or 35 mm plates for imaging (Nest Biotechnology Co, Wuxi, Jiangsu, China, Cat. No: 706001) at 37°C in a humidified incubator with 5% CO_2. Cells were cultured until they reached approximately 70% confluence.

Cell Staining. To perform nuclei staining for cell counting and in the original workflow, 10 µL of 6.5 mM saponin (Sigma-Aldrich, St. Louis, MO, USA, Cat. No:8047152) and 5 µL of 1 mM propidium iodide (PI, Sigma-Aldrich, St. Louis, MO, USA, Cat. No:25535164) were added into the Hanks' Balanced Salt Solution (HBSS) (Gibco, Grand Island, NY, USA, Cat. No:14025092) after completion of the time-lapse experiment (see CRRC Experimental flow for more details).[14] After 10 min, cells were imaged with no washing. For experiments that required cytoplasmic staining; cells were treated with a 2 µM DRAQ9 solution (Novus Biologicals, Littleton, CO, USA, Cat. No: NBP2-81128) in HBSS. After 30 min, cells were washed three times with PBS (Cytiva, Logan, Utah, USA, Cat. No: SH30256.01) and then imaged.

CRRC Experimental Flow. Each CRRC experiment was conducted on a dish with a 35-mm diameter. Cells were cultured on larger dishes (60 or 100 mm) and then split and placed on 35-mm-diameter dishes, as needed. At this point, to prepare cells for a full CRRC cross-membrane transport experiment, we performed the following six steps. First, we removed culture medium and washed cells once with 1 mL of PBS. Second, we incubated cells for 30 min in 1.2 mL of HBSS containing 1.5 µM fluorescein (Sigma-Aldrich St. Louis, MO, USA, Cat. No:518478), the substrate of cross-membrane transport, and 10 µM glibenclamide (Research Biochemicals International, Natick, MA, USA Cat. No: G106), a multidrug resistance transport inhibitor. Third, we removed HBSS, and washed cells three times with 1 mL of PBS. Fourth, we added 1.2 mL of HBSS and started image acquisition with alternating fluorescence and BF modes every 1 min for 1 h.

Image Acquisition. In the past CRRC studies, imaging was performed with confocal laser-scanning fluorescence microscopy.[12, 15, 16] In the current work, we used epifluorescence microscopy with a Leica DMi8 high-throughput cell-imaging system. This imager allows carrying out fully automated time-lapse image acquisition with alternating fluorescence and transmitted-light microscopy. Images were acquired with a 10× objective lens and the fluorescence of intracellular fluorescein was excited with a blue light-emitting diode. A FITC filter cube was used for fluorescein, RHOD cube for nuclei stain PI, and a Cy5 cube was used for cytoplasmic stain DRAQ9. For transmitted-light microscopy, BF and DIC images were acquired with the same 10× objective lens as fluorescence. PC images were acquired with a N Plan 10×/0.25 PH1 objective lens. All images were captured with a deep-cooled high resolution sCMOS camera. See Note S1 for details on microscope settings and microscopy protocol.

Image Processing Software. We chose Fiji,[17] an open-source software, because it supports all image processing and image analysis required for our workflow: (*i*) merging fluorescence and brightfield images, (*ii*) cell segmentation, *i.e.*, determination of cell contours and, thus, identification of cells using the StarDist dectector,[18] (*iii*) cell tracking including creation of tracks and exclusion of cells with incomplete tracks, and (*iv)* integration of intracellular fluorescence withing the cell contours. Advantageously, a recent version of the Fiji's plugin named TrackMate integrates capabilities for steps (*ii*) – (*iv)*, which greatly simplifies image processing and analysis.[19] Software settings and other details can be found in Note S2.

Extraction and Analysis of Kinetic Traces. Intracellular fluorescence intensities were extracted from TrackMate and arranged on Microsoft Excel to build individual kinetic traces. The kinetic traces were placed in OriginPro software and exponentially fitted with the "ExpDec1" function from the time of medium exchange at the beginning of the experiment (initiation of cross-membrane transport). In the past CRRC studies, we determined a rate constant characterizing the activity of ATP-binding cassette (ABC) transporters, k_{MDR}. Here, we determined a rate constant of total substrate efflux, k_{efflux}. The main reason for this change was that total drug extrusion by all mechanisms of cross-membrane transport may be more relevant to drug resistance than transport catalyzed by ABC transporters only. In addition, the determination of k_{efflux} is simpler experimentally than that of k_{MRD}. The k_{efflux} rate constants were obtained from cells that passed exponential fitting; negative values of k_{efflux} and all k_{efflux} values with high uncertainty (RSD > 100%) were removed from further analysis.

Cell Population Analysis. Cross-membrane transport of each cell population was characterized by histograms of k_{efflux} values of individual cells. Histograms were plotted in OriginPro software using the Custom Binning mode and were characterized by the median (peak position) and skewness (peak asymmetry) values obtained with the Descriptive Statistics tool. The comparison of distributions was conducted using the Kolmogorov-Smirnov test, considering $\alpha = 0.001$ as a criterion of statistical significance.

RESULTS AND DISCUSSION

Need for Transmitted Light Microscopy. The first key requirement for ensuring CRRC insensitivity to cell movement is that cell contours be identified in each fluorescence image in the time-stack of images (cell contours can be determined automatically with the Fiji software used in this study). The very nature of CRRC does not allow using fluorescence from the substrate (product) of the studied reaction for the identification of cell contours. The reason is that CRRC follows kinetics of fluorescence decrease (or increase), and, therefore, a part of fluorescence images in the time-stack always has too weak intracellular fluorescence for cell contour identification. The only apparently feasible way of identifying cell contours in each fluorescence image is to take an accompanying high-contrast image right after each fluorescence image of the substrate (product).

The accompanying image can be either a fluorescence one or a

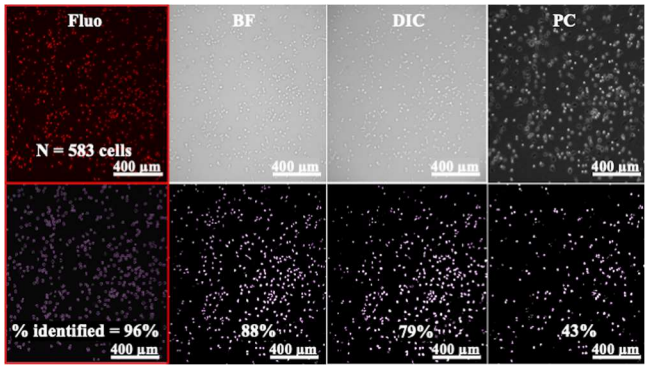

Figure 2. Comparing three modes of transmitted light-microscopy (BF, DIC, and PC) for the purpose of cell contour determination. Correct cell identification was used as a criterion for decision making. Fluorescence microscopy (Fluo) of TOV-112D cells stained with propidium iodide was used as a reference method (images in red frame). Cells were manually counted in the fluorescence image, and this number (583) was used as a reference. The four images on the top were converted into high-contrast images (see text for details) and loaded onto the cell-contour identification software. The images at the bottom show an overlay of the top images with the determined cell contours (magenta). The numbers show percentages of correctly identified cells in the four images.

transmitted-light one. Using an accompanying fluorescence image necessitates cells' pre-staining with a fluorescence probe spectrally different from the substrate (product). Such a probe would impose an additional chemical stress on the cells and could also interfere with measurements of substrate (product) fluorescence intensity due to unavoidable spectral overlaps. Therefore, our *a priori* preference is an accompanying transmitted light image.

Further, transmitted light images can be modified to have a limited pixel intensity range, so that pixels with intensities above the upper threshold limit will convert to white, and pixels with intensities below the lower threshold limit will convert to black. By limiting the pixel intensity range, this procedure essentially converts a traditional transmitted light image into a high-contrast image. In this modified image, cells appear as bright spots on a black background. Accordingly, cell contours are more easily identifiable by the human eye, making this modified image favourable for automated cell contour identification. Thus, the modified transmitted light image will be used for cell contour identification and cell tracking through the time-stack of images.

Preferred Mode of Transmitted light Microscopy. There are three major modes of transmitted-light microscopy: bright field (BF), differential interference contrast (DIC), and phase contrast (PC). We decided to find the most suitable one by comparing their performance in cell-contour determination. The performance can be assessed using two criteria: 1) correct identification of cells and 2) accurate and precise determination of cell contours. As a reference method to identify cells, we used manual counting of cells contrasted with PI. PI is a bright fluorescent dye that stains nuclei in permeabilized cells. The nuclei are always spaced out by the cytoplasm; therefore, fluorescence images of propidium iodide-stained cells appear as well separated bright spots in a mono-layer cell culture. Such images are well suitable for manual cell counting (a cumbersome task) and for computer assisted cell counting.[20]

We took three consecutive transmitted light images of TOV-112D cells: BF, DIC, and PC (Figure 2). To obtain the desired images for cell identification, we first focused on cells in each imaging mode, lowered the objective lens by approximately 30 µm for cells to appear as white objects, and then adjusted the intensity threshold to remove the background. This process was repeated for every imaging mode (see Note S1 for details). For the fluorescence image, we permeabilized cells with saponin and stained their nuclei

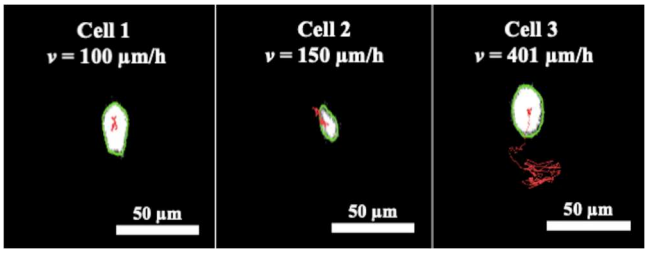

Figure 3. Determination of velocities of motile (TOV-112D) cells from cell tracks obtained with high frequency time-lapse BF imaging (1 image per 10 s). The three panels show representative cells with different levels of motility; red lines show respective tracks. Cell contours (green) show cell positions at the beginning of time-lapse imaging. Average velocities are shown in the panels.

with propidium iodide. The cells were counted manually throughout the entire field of view in the fluorescence image, and this number was used as a reference. The cells were then counted with the cell-contour determination software (StarDist) in all four images and compared to the reference number. A radius range filter (3 to 12 µm) was applied to all four images to ensure we counted single cells by excluding cell debris and cells in clusters that could not be distinguished. We found that the software could identify $98 \pm 1\%$ (expectedly), $83 \pm 5\%$, $68 \pm 8\%$, and $47 \pm 4\%$ in fluorescence, BF, DIC, and PC images, respectively. Thus, we selected to use modified BF images for cell contour identification and tracking.

Assumption of Cell Immobility During Acquisition of Two Consecutive Images. There is a short but finite time interval of a few seconds between a fluorescence image and an accompanying BF image in our new workflow. We evaluated to what extent cell movement during this short time period could affect the results of CRRC. We performed time-lapse imaging of highly motile cells with high frequency of image acquisition for recording cell tracks (Figure 3). By using the migration tracks, we found that the velocity of cell migration did not follow normal distribution (Note S3). The peak of the distribution was at approximately 150 µm/h and the interquartile range was 40 µm/h. The fastest cell in the image had a velocity of $v \approx 401$ µm/h. A maximum time gap between acquiring adjacent fluorescence and BF images is approximately $t_1 = 3.0$ s. The average shift of the fastest cell during this short time is $x = vt_1 = 0.33$ µm while the cell diameter was $d = 13 \pm 3$ µm. The error that such a shift in cell position can cause in the integration of intracellular fluorescence intensity over the area within cell contours is of the order of $x/d \approx 0.025$ (see Note S4). Accordingly, the error in intracellular fluorescence intensity introduced by a finite time interval between the fluorescence image and the accompanying BF image is approximately 2.5%, *i.e.*, negligible, even for the fastest moving cells. Therefore, cell positions in these images can be assumed to be identical.

Consideration on Focusing. On one hand, the quality of focusing in fluorescence images can affect the determination of intracellular fluorescence intensity. On the other hand, fluorescence cannot be used for focusing cells when the substrate is fluorogenic as fluorescence intensity in the initial images of the time-lapse series is certainly too low for focusing. An obvious solution is using a BF image for focusing; however, the focal plane in the fluorescence image is higher than in the BF image. Advantageously, the distance between the focal planes in BF and fluorescence images is near the cell diameter, which is roughly 10 µm for a typical tissue cell.[21] Therefore, an approximate position of the focal plane in the fluorescence image can be found by simply raising the objective lens by 10 µm. Since this is only an approximate position, the question arises how sensitive the

determination of intracellular fluorescence intensity is to a deviation from the real focal plane in the fluorescence image.

To answer this question, we performed the following experiment. We stained cells with the cytoplasmic probe DRAQ9. An in-focus BF image was taken first and used for cell contours determination. Then, we focused on the cells in the fluorescence mode and found that the fluorescence focal plane was ~10 µm above the BF focal plane. We took fluorescence images with four positions of the objective lens: –5, 0, 5, and 10 µm (0 corresponds to the in-focus position in the fluorescence image). Intracellular fluorescence intensities were found in all fluorescence images using the cell contours determined from the BF image. Fluorescence intensities for cells in the in-focus image were used as references to find relative deviations in fluorescence intensities for the out-of-focus images: $-2.2 \pm 5.8\%$, $3.85 \pm 9.1\%$, and $8.5 \pm 12.2\%$ for –5, 5, and 10 µm, respectively (see Note S5 for details). These results suggest that intracellular fluorescence intensity is almost insensitive to focusing for a wide range of objective lens positions. Accordingly, fluorescence images can be taken simply with a lens position of one cell diameter above the lens position corresponding to focus in the BF mode.

Testing the New CRRC Workflow. The new and original workflows are schematically depicted in Figure 4. We wanted to compare these two workflows and establish their sensitivity to cell motility. To do so, we performed a CRRC study of cross-membrane transport in TOV cells. It is noteworthy that, to favour accurate cell tracking in the new workflow, we set the time gap between adjacent BF images (t_2) to be shorter than the time required for the fastest cell (with velocity v) to cover a distance equal to a typical cell diameter d: $t_2 << d/v$. Hence, using the values of $v = 401$ µm/h and $d = 13$ µm, we set $t_2 = 1$ min (see section "Assumption of Cell Immobility During Acquisition of Two Consecutive Images" above). Then, the two workflows were used to process the time-lapse images in parallel and obtain time dependencies (kinetic curves) of fluorescence intensities for individual cells, which can be found in kineticcurves.zip. Kinetic curves were fitted with a single exponential function to find the unimolecular rate constant k_{efflux} for every single cell. The results of the exponential fitting are archived in fitting.zip.

To examine the sensitivity of both workflows to cell motility, we examined the kinetics corresponding to cells with low and high motility — total paths traveled were below 20 µm and above 40 µm, respectively. We found that the two workflows expectedly produced similar values of k_{efflux} for the low-motility cells (see example in Figure 5A). This result served as cross-validation for the two workflows. On the contrary, the two workflows returned drastically different k_{efflux} values for the high-motility cells (see example in Figure 5B). The new workflow recorded expected k_{efflux} values since high motility cells were followed (a movie showing this event can be found in newworfklowvideo.zip). However, the original workflow recorded a much faster fluorescence decay for highly-motile cells. This decay should be ascribed to such cells' moving out of the cell-contour mask used for fluorescence integration (a movie demonstrating this phenomenon can be found in originalworkflowvideo.zip). The faster the cell leaves the mask – the greater the apparent k_{efflux}. In some cases, exponential fitting fails for such cells but in many cases the fitting returns a constant which is a great overestimate of the real k_{efflux} value.

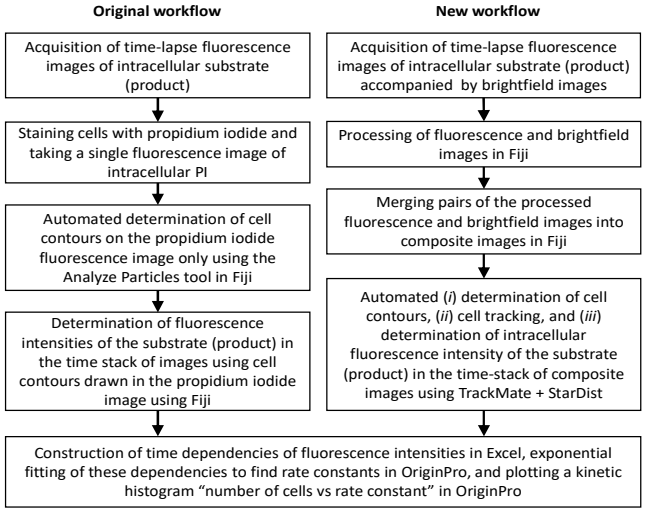

Figure 4. Schematic depictions of the original (left) and new (right) workflows. The last step is identical for both workflows.

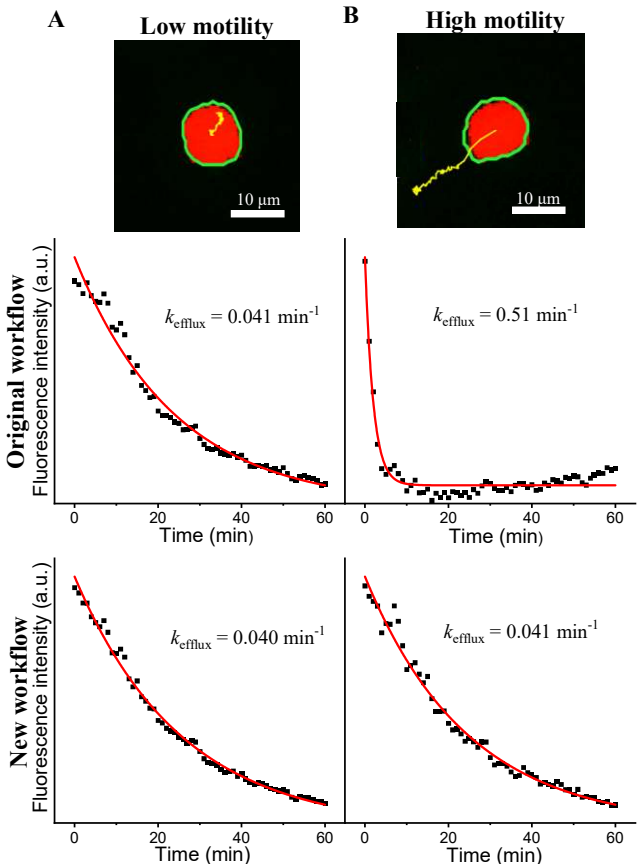

Figure 5. Examples of kinetics obtained using the original and new workflows for **(A)** low-motility cell; in this case, the two workflows compute almost identical kinetics and k_{efflux} values and **(B)** high-motility cell; here, the two workflows compute drastically different kinetics and k_{efflux} values (12-fold difference)

An important conclusion from the detailed comparison of fluorescence-decay kinetics of cells with different motility is that the original workflow tends to overestimate the rate constant of substrate efflux for highly-motile cells. This necessarily leads to the shift of the CRRC histogram produced by the original workflow to the right when compared to the histogram obtained with the new workflow (Figure 6). We examined whether the histograms produced by the two workflows are different by using a non-parametric statistical test of the equality of the two distributions. The Kolmogorov-Smirnov test confirmed that the histograms in Figure 6 differed significantly at the 0.001 significance level ($D = 0.420$, $D_\alpha = 0.209$, $p = 6.32 \times 10^{-14}$, see Note S6 for more details on statistics). It is noteworthy to mention that the two distributions in Figure 6 have different sample sizes. This occurs since the two workflows differ in the cell-segmentation step. Nevertheless, the Kolmogorov-Smirnov test is insensitive to differences in sample size. Therefore, based on these results we can conclude that the new workflow is insensitive to cell motility and can be used for CRRC analysis of a wide scope of cell types.

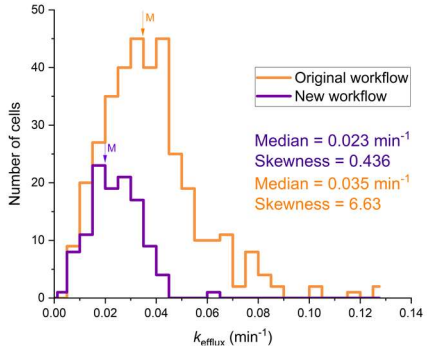

Figure 6. CRRC final histograms of cross-membrane transport activity in TOV-112D cells. The variation in sample size is due to differences in cell-segmentation and filtering processes. Median and skewness values are shown; positions of medians are with arrows. The histogram obtained from the original workflow is clearly skewed towards the right. The two distributions were found to be statistically different by the Kolmogorov-Smirnov test at the 0.001 significance level ($p = 6.32 \times 10^{-14}$).

CONCLUDING REMARKS

The developed workflow is an important move towards CRRC becoming a practical analytical tool. This workflow will allow researchers to address multiple challenges in tissue-sample handling and start CRRC studies of reactions other than MDR. In recent years, there has been significant progress in rational design of high-quality fluorogenic substates for intracellular enzymes. Specifically, such substrates have been created for enzymes responsible for chemoresistance of cancer tissues: aldehyde dehydrogenase,[22, 23] and cytochrome P450.[24] We foresee that using CRRC along with these substrates will help discover and validate new types of predictive biomarkers of chemoresistance.[13]

REFERENCES

(1) Kwon, M. J.; Shin, Y. K. Regulation of ovarian cancer stem cells or tumor-initiating cells. *Int J Mol Sci* **2013**, *14* (4), 6624-6648. DOI: 10.3390/ijms14046624.

(2) McIntosh, K.; Balch, C.; Tiwari, A. K. Tackling multidrug resistance mediated by efflux transporters in tumor-initiating cells. *Expert Opin Drug Metab Toxicol* **2016**, *12* (6), 633-644. DOI: 10.1080/17425255.2016.1179280.

(3) Lee, H. E.; Kim, J. H.; Kim, Y. J.; Choi, S. Y.; Kim, S. W.; Kang, E.; Chung, I. Y.; Kim, I. A.; Kim, E. J.; Choi, Y.; et al. An increase in cancer stem cell population after primary systemic therapy is a poor prognostic factor in breast cancer. *Br J Cancer* **2011**, *104* (11), 1730-1738. DOI: 10.1038/bjc.2011.159.

(4) Ayob, A. Z.; Ramasamy, T. S. Cancer stem cells as key drivers of tumour progression. *J Biomed Sci* **2018**, *25* (1), 20. DOI: 10.1186/s12929-018-0426-4.

(5) Mantzaris, N. V. From single-cell genetic architecture to cell population dynamics: quantitatively decomposing the effects of different population heterogeneity sources for a genetic network with positive feedback architecture. *Biophys J* **2007**, *92* (12), 4271-4288. DOI: 10.1529/biophysj.106.100271.

(6) Kubitscheck, U.; Pratsch, L.; Passow, H.; Peters, R. Calcium pump kinetics determined in single erythrocyte ghosts by microphotolysis and confocal imaging. *Biophys J* **1995**, *69* (1), 30-41. DOI: 10.1016/S0006-3495(95)79875-7.

(7) Sunray, M.; Zurgil, N.; Shafran, Y.; Deutsch, M. Determination of individual cell Michaelis-Menten constants. *Cytometry* **2002**, *47* (1), 8-16. DOI: 10.1002/cyto.10029.

(8) Koshkin, V.; Krylov, S. N. Single-cell-kinetics approach to compare multidrug resistance-associated membrane transport in subpopulations of cells. *Anal Chem* **2011**, *83* (16), 6132-6134. DOI: 10.1021/ac201690t.

(9) Koshkin, V.; Krylov, S. N. Correlation between multi-drug resistance-associated membrane transport in clonal cancer cells and the cell cycle phase. *PLoS One* **2012**, *7* (7), e41368. DOI: 10.1371/journal.pone.0041368.

(10) Koshkin, V.; Krylov, S. N. Single-cell-kinetics approach to discover functionally distinct subpopulations within phenotypically uniform populations of cells. *Anal Chem* **2013**, *85* (5), 2578-2581. DOI: 10.1021/ac400151v.

(11) Koshkin, V.; Yang, B. B.; Krylov, S. N. Kinetics of MDR transport in tumor-initiating cells. *PLoS One* **2013**, *8* (11), e79222. DOI: 10.1371/journal.pone.0079222.

(12) Koshkin, V.; Kochmann, S.; Sorupanathan, A.; Peng, C.; Ailles, L. E.; Liu, G.; Krylov, S. N. Cytometry of Reaction Rate Constant: Measuring Reaction Rate Constant in Individual Cells To Facilitate Robust and Accurate Analysis of Cell-Population Heterogeneity. *Anal Chem* **2019**, *91* (6), 4186-4194. DOI: 10.1021/acs.analchem.9b00388.

(13) Bleker de Oliveira, M.; Koshkin, V.; Liu, G.; Krylov, S. N. Analytical Challenges in Development of Chemoresistance Predictors for Precision Oncology. *Anal Chem* **2020**, *92* (18), 12101-12110. DOI: 10.1021/acs.analchem.0c02644.

(14) Yeh, C. J.; Hsi, B. L.; Faulk, W. P. Propidium iodide as a nuclear marker in immunofluorescence. II. Use with cellular identification and viability studies. *J Immunol Methods* **1981**, *43* (3), 269-275. DOI: 10.1016/0022-1759(81)90174-5.

(15) Koshkin, V.; Bleker de Oliveira, M.; Peng, C.; Ailles, L. E.; Liu, G.; Covens, A.; Krylov, S. N. Spheroid-Based Approach to Assess the Tissue Relevance of Analysis of Dispersed-Settled Tissue Cells by Cytometry of the Reaction Rate Constant. *Anal Chem* **2020**, *92* (13), 9348-9355. DOI: 10.1021/acs.analchem.0c01667.

(16) Koshkin, V.; De Oliveira, M. B.; Peng, C.; Ailles, L. E.; Liu, G.; Covens, A.; Krylov, S. N. Multi-drug-resistance efflux in cisplatin-naive and cisplatin-exposed A2780 ovarian cancer cells responds differently to cell culture dimensionality. *Mol Clin Oncol* **2021**, *15* (2), 161. DOI: 10.3892/mco.2021.2323.

(17) Schindelin, J.; Arganda-Carreras, I.; Frise, E.; Kaynig, V.; Longair, M.; Pietzsch, T.; Preibisch, S.; Rueden, C.; Saalfeld, S.; Schmid, B.; et al. Fiji: an open-source platform for biological-image analysis. *Nat Methods* **2012**, *9* (7), 676-682. DOI: 10.1038/nmeth.2019.

(18) Schmidt, U.; Weigert, M.; Broaddus, C.; Myers, G. Cell Detection with Star-Convex Polygons. Cham, 2018; Springer International Publishing: pp 265-273.

(19) Tinevez, J. Y.; Perry, N.; Schindelin, J.; Hoopes, G. M.; Reynolds, G. D.; Laplantine, E.; Bednarek, S. Y.; Shorte, S. L.; Eliceiri, K. W. TrackMate: An open and extensible platform for single-particle tracking. *Methods* **2017**, *115*, 80-90. DOI: 10.1016/j.ymeth.2016.09.016.

(20) Chan, L. L.; Smith, T.; Kumph, K. A.; Kuksin, D.; Kessel, S.; Déry, O.; Cribbes, S.; Lai, N.; Qiu, J. A high-throughput AO/PI-based cell concentration and viability detection method using the Celigo image cytometry. *Cytotechnology* **2016**, *68* (5), 2015-2025. DOI: 10.1007/s10616-016-0015-x.

(21) Del Monte, U. Does the cell number 109 still really fit one gram of tumor tissue? *Cell Cycle* **2009**, *8* (3), 505-506. DOI: 10.4161/cc.8.3.7608.

(22) Anorma, C.; Hedhli, J.; Bearrood, T. E.; Pino, N. W.; Gardner, S. H.; Inaba, H.; Zhang, P.; Li, Y.; Feng, D.; Dibrell, S. E.; et al. Surveillance of Cancer Stem Cell Plasticity Using an Isoform-Selective Fluorescent Probe for Aldehyde Dehydrogenase 1A1. *ACS Central Science* **2018**, *4* (8), 1045-1055. DOI: 10.1021/acscentsci.8b00313.

(23) Bearrood, T. E.; Aguirre-Figueroa, G.; Chan, J. Rational Design of a Red Fluorescent Sensor for ALDH1A1 Displaying Enhanced Cellular Uptake and Reactivity. *Bioconjugate Chemistry* **2020**, *31* (2), 224-228. DOI: 10.1021/acs.bioconjchem.9b00723.

(24) Chang, T. K.; Waxman, D. J. Enzymatic analysis of cDNA-expressed human CYP1A1, CYP1A2, and CYP1B1 with 7-ethoxyresorufin as substrate. *Methods Mol Biol* **2006**, *320*, 85-90. DOI: 10.1385/1-59259-998-2:85.

SUPPORTING INFORMATION
Making Cytometry of Reaction Rate Constant (CRRC) Applicable to Motile Cells

Robel Yosief,[1#] Giammarco Nebbioso,[1#] Vasilij Koshkin,[1] Yumin Qiu,[2] Chun Peng,[2] Vadim Elisseev,[3] and Sergey N. Krylov*[1]

[1] Department of Chemistry and Centre for Research on Biomolecular Interactions, York University, Toronto, Ontario M3J 1P3, Canada;
[2] Department of Biology and Centre for Research on Biomolecular Interactions, York University, Toronto, Ontario M3J 1P3, Canada;
[3] IBM Research Europe, The Hartree Centre, , Daresbury Laboratory, Warrington, WA4 2AD, UK and Wrexham Glyndwr University, Mold Rd, Wrexham LL11 2AW, UK

#These authors contributed equally

*Corresponding author's email: skrylov@yorku.ca

TABLE OF CONTENT

Additional supplementary files

File name and description

- images.zip
    - It contains raw images for:
        - Figure 2 (main text); the main folder contains three subfolders named 'region X'. Each region represents a different *x*-*y* position of the cell plate. Each 'region X' folder contains images that were obtained in BF, DIC and PC mode, respectively.
        - Figure 3 (main text); it contains raw images for the time lapse experiment. The time interval between each image is 10 s.
        - Figure 6 (main text); it contains the set of adjacent BF and fluorescent images obtained during the CRRC experiment. The time interval between the images in the BF folder is 1 min. The time interval between the images in the Fluo folder is 1 min. The folder also contains an image named 'PI'. This image reveals the position of each single cell at the end of the CRRC experiment upon PI staining, and it is used in the original workflow.
        - Figure S3 (SI); this folder contains two in-focus BF images: the raw image and the image after threshold was applied. It also contains the in-focus and out-of-focus (5 µm below, 5 µm above, and 10 µm above the in-focus position, respectively) fluorescence images.
- kinetictraces_and_fittingresults.zip
    - It contains two different .csv files. One is named 'Kinetic traces_and_fittingresults_new workflow' and the other one is named 'Kinetic traces_and_fittingresults_original workflow'. Both files contain one sheet displaying the fluorescence intensity values as a function of time for individual cells. It also contains the equation used for fitting and the fitting results computed by OriginPro (scroll down to line 69).
- Trackingvideos.zip
    - It contains two videos. Each video shows the cell movement of the same single cell over the course of a time-lapse experiment of 1 hour duration, with a 1 min time interval. The 'newworkflowvideo' shows the ability of the new workflow to track the cell's movements over time. The 'oldworkflowvideo' shows the absence of tracking, leading to an incorrect integration of fluorescence intensity over time for the same single cell (which subsequently results in the overestimation of k_{efflux})

Note S1: Microscope Settings and Protocol

Imaging was performed with a Leica DMi8 high-throughput cell-imaging system. Four modes were used: fluorescence, brightfield (BF), differential interference contrast (DIC), and phase contrast (PC). The Mark and Find feature of the microscope was used to acquire images of multiple regions of the cell plate and the Relative Focus Correction feature was used to set different Z-positions between the fluorescence and BF channels. Image settings for each figure are shown below:

Figure 2 in the main text

- BF: no binning, 7.81 ms exposure, high well capacity, intensity 48, aperture 7, transmitted light field diaphragm (Tl-Fld) 23, 196–191 intensity threshold
- DIC: no binning, 7.81 ms exposure, high well capacity, intensity 128, aperture 15, Tl-Fld 46, bias 50, 192–192 intensity threshold
- PC: no binning, 7.81 ms exposure, high well capacity, intensity 130, aperture 24, Tl-Fld 23, 129–128 intensity threshold
- Fluorescence: RHOD channel, no binning, 50 ms exposure, low noise, fluorescence intensity manager (FIM) 30%, incident light field diaphragm (Il-Fld) 6

Figure 3 in the main text

- BF: no binning, 8 ms exposure, high well capacity, intensity 48, aperture 11, Tl-Fld 46, 84–80 intensity threshold

Figures 6 and 7 in the main text

- BF: no binning, 7.81 ms exposure, high well capacity, intensity 38, aperture 12, Tl-Fld 46, 196–191 intensity threshold
- Fluorescence: FITC channel, no binning, 7.81 ms exposure, low noise, FIM: 30%, Il-Fld 6

Figure S3 in the supporting information

- BF: no binning, 7.81 ms exposure, high well capacity, intensity 48, aperture 7, Tl-Fld 23, 196-191 intensity threshold
- Fluorescence: Y5 channel, 2×2 binning, 50 ms exposure, low noise, FIM 30%, Il-Fld 6

Note S2: Fiji and TrackMate Detailed Workflow

Here we explain the new workflow step-by-step. The time-lapse fluorescence and BF images, which are archived in images.zip, were evaluated in nine steps, as shown below. Image processing was conducted using the Fiji software (https://imagej.net/software/fiji/). Cells were tracked with TrackMate (version 7.6.1; https://imagej.net/plugins/trackmate/), an open-source plugin available on Fiji.

1. Load both sets of images (BF and Fluo) onto Fiji

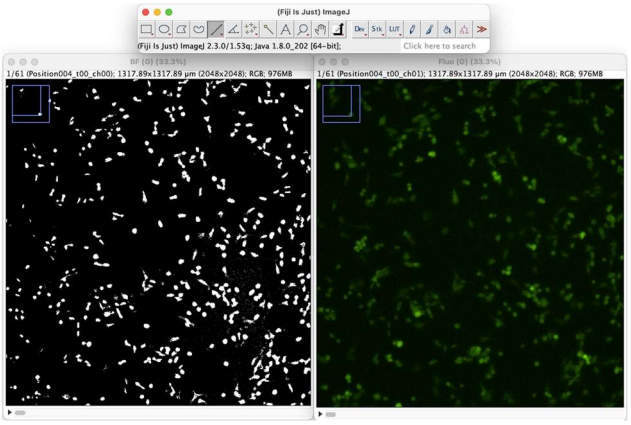

2. Merge the BF and Fluo images as a composite. Assign BF as Channel 1 and Fluo as Channel 2

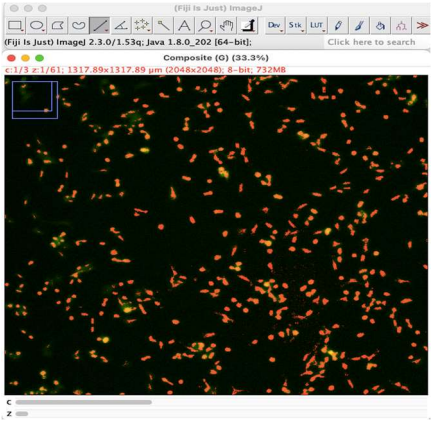

3. Use the Fiji plugin TrackMate on the composite channel

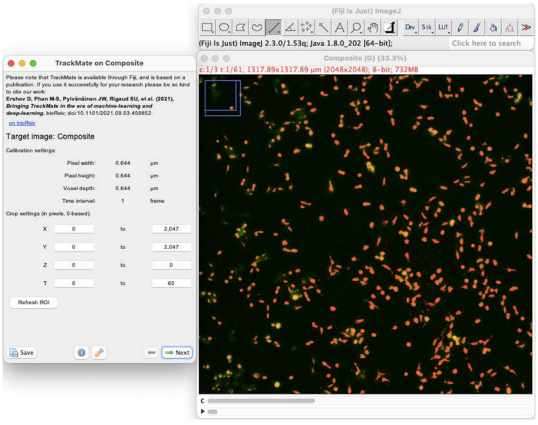

4. Select StarDist detector for cell segmentation on channel 1 (BF)

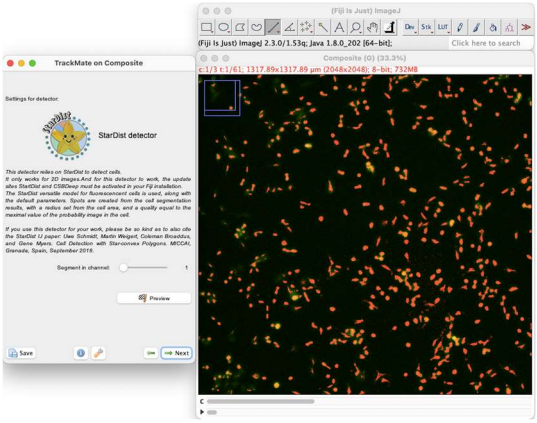

5. Apply radius range filter

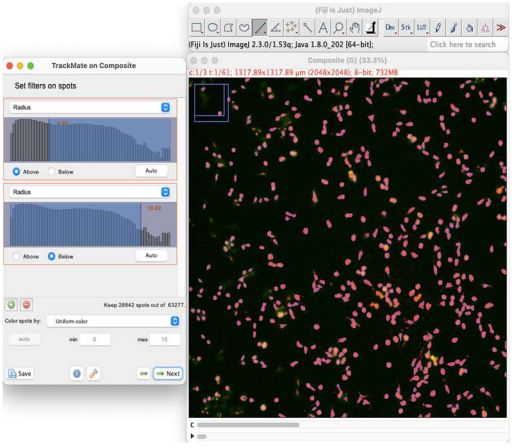

6. Select LAP tracker for cell tracking

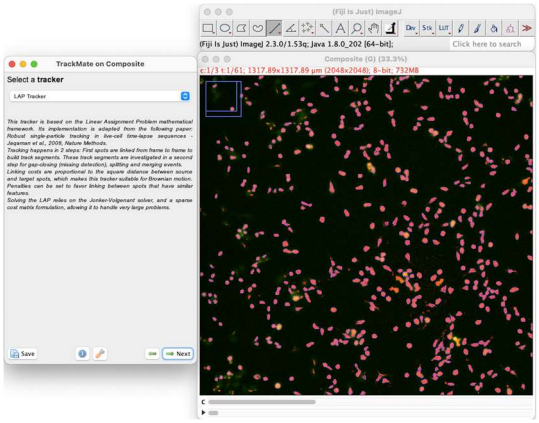

7. Enter max distance that cells can travel between frames (~ cell diameter) and do NOT allow gap closing, merging, or splitting

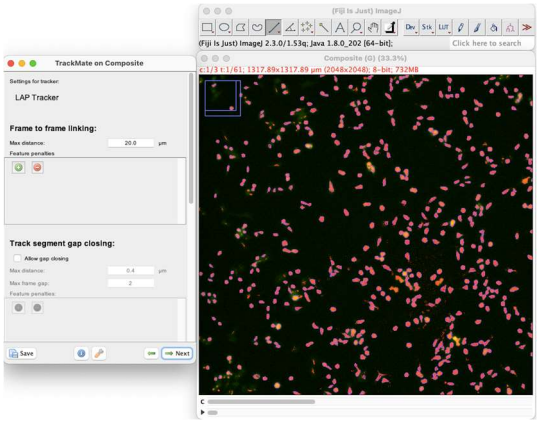

8. Filter the generated cell tracks by the duration of track, include only full-length tracks

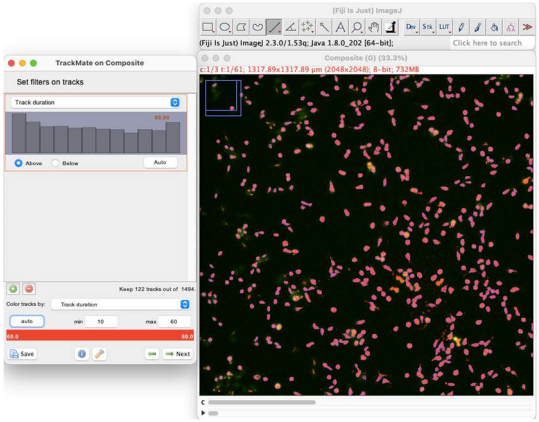

9. Open “Track tables” and select spots tab. Adjust Track IDs (cells) column so that cells are sequentially ordered by frame # and click export to CSV. In the CSV file, only the “Track ID” and “Mean Intensity Channel 2” columns are kept (highlighted red).

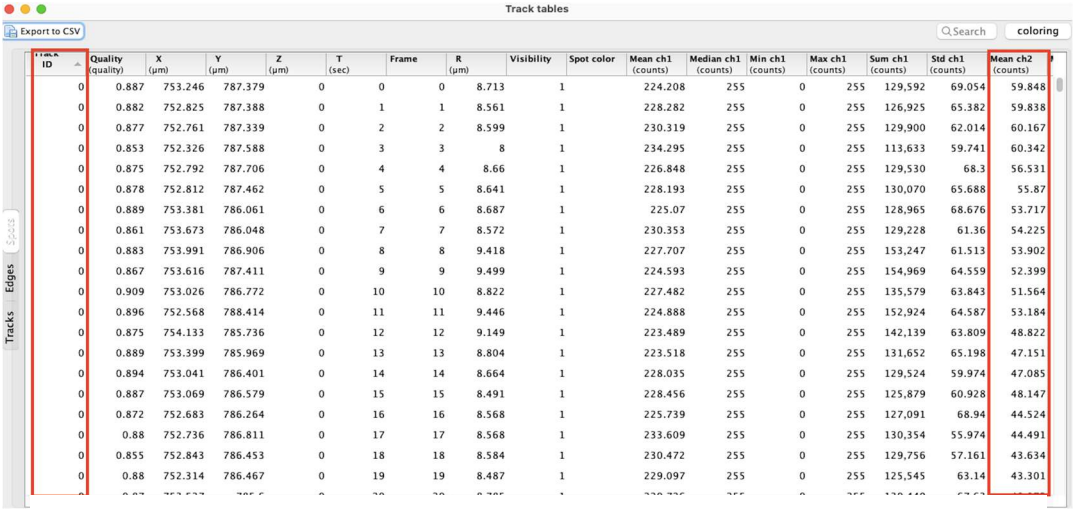

ID	Quality (quality)	X (µm)	Y (µm)	Z (µm)	T (sec)	Frame	R (µm)	Visibility	Spot color	Mean ch1 (counts)	Median ch1 (counts)	Min ch1 (counts)	Max ch1 (counts)	Sum ch1 (counts)	Std ch1 (counts)	Mean ch2 (counts)
0	0.887	753.246	787.379	0	0	0	8.713	1		224.208	255	0	255	129,592	69.054	59.848
0	0.882	752.825	787.388	0	1	1	8.561	1		228.282	255	0	255	126,925	65.382	59.838
0	0.877	752.761	787.339	0	2	2	8.599	1		230.319	255	0	255	129,900	62.014	60.167
0	0.853	752.326	787.588	0	3	3	8	1		234.295	255	0	255	113,633	59.741	60.342
0	0.875	752.792	787.706	0	4	4	8.66	1		226.848	255	0	255	129,530	68.3	56.531
0	0.878	752.812	787.462	0	5	5	8.641	1		228.193	255	0	255	130,070	65.688	55.87
0	0.889	753.381	786.061	0	6	6	8.687	1		225.07	255	0	255	128,965	68.676	53.717
0	0.861	753.673	786.048	0	7	7	8.572	1		230.353	255	0	255	129,228	61.36	54.225
0	0.883	753.991	786.906	0	8	8	9.418	1		227.707	255	0	255	153,247	61.513	53.902
0	0.867	753.616	787.411	0	9	9	9.499	1		224.593	255	0	255	154,969	64.559	52.399
0	0.909	753.026	786.772	0	10	10	8.822	1		227.482	255	0	255	135,579	63.843	51.564
0	0.896	752.568	788.414	0	11	11	9.446	1		224.888	255	0	255	152,924	64.587	53.184
0	0.875	754.133	785.736	0	12	12	9.149	1		223.489	255	0	255	142,139	63.809	48.822
0	0.889	753.399	785.969	0	13	13	8.804	1		223.518	255	0	255	131,652	65.198	47.151
0	0.894	753.041	786.401	0	14	14	8.664	1		228.035	255	0	255	129,524	59.974	47.085
0	0.887	753.069	786.579	0	15	15	8.491	1		228.456	255	0	255	125,879	60.928	48.147
0	0.872	752.683	786.264	0	16	16	8.568	1		225.739	255	0	255	127,091	68.94	44.524
0	0.88	752.736	786.811	0	17	17	8.568	1		233.609	255	0	255	130,354	55.974	44.491
0	0.855	752.843	786.453	0	18	18	8.584	1		230.472	255	0	255	129,756	57.161	43.634
0	0.88	752.314	786.467	0	19	19	8.487	1		229.097	255	0	255	125,545	63.14	43.301

The CSV file is then opened in Microsoft Excel, the time dependencies of fluorescence intensities (kinetic traces) for each cell are arranged to be side-by-side for exponential fitting. The CSV files containing the traces can be found in kinetictraces.zip

Note S3: Distribution of Cell Migration Velocity

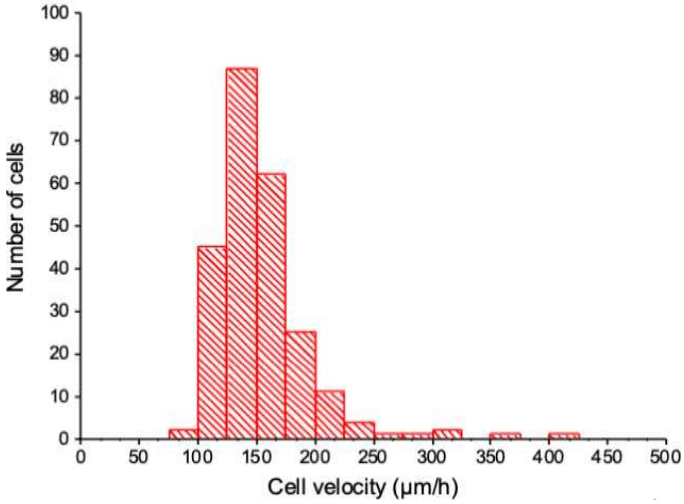

Figure S1. Distribution of cell migration velocities (μm/h) found by high frequency (1 image per 10 s) time-lapse BF imaging. The distribution was not normal according to the Shapiro-Wilks normality test at the 0.05 level ($P = 2.2 \times 10^{-16}$). The peak of the distribution was approximately 150 μm/h with an interquartile range of 40 μm/h. The fastest cell had a velocity of 401 μm/h

Note S4: Determination of Error in Fluorescence Intensity Integration Caused by a Shift in Cell Position from the Fluorescence Image and Accompanying BF Image

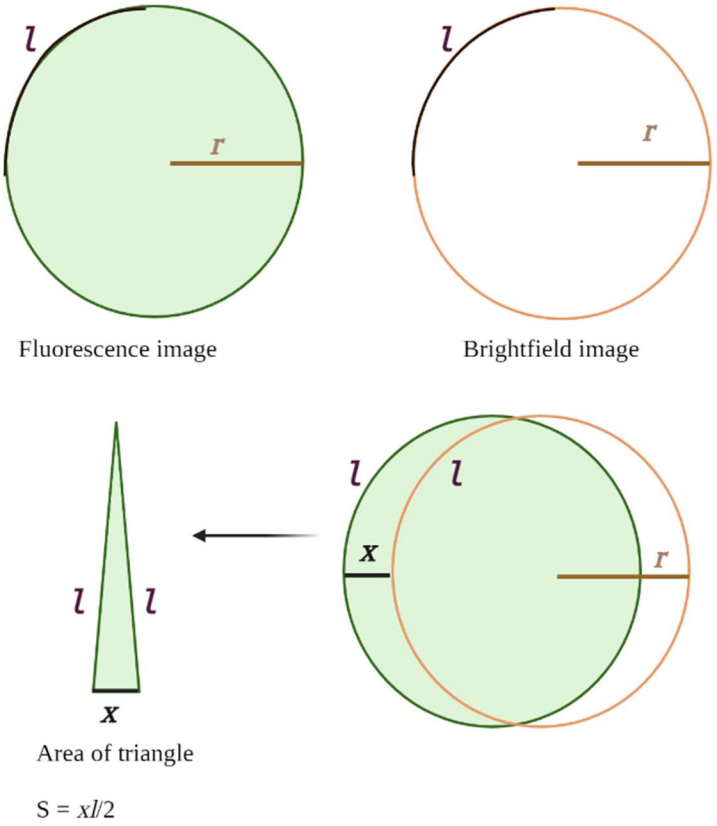

Figure S2. Schematic representation of the effects of cellular movements on fluorescence integration. Let's assume that $x/r << 1$, where x is the distance travelled by the cell and r is a cell radius. In this case, the area of the lune encompassing x can be approximated by that of a triangle: $s = xl/2$. The total area that is excluded from the overlap of the two circles is $S = 2s = 2xl/2 = xl = x(2\pi r/4) = \pi xr/2$. The area of the circle is: $S_{circle} = \pi r^2$. The area of the shape of overlap of the two circles is the one that will be used for fluorescence intensity determination. It is smaller than the area of a single circle by S. The relative error of circle area determination is: $\Delta S = S/S_{circle} = \pi xr/(2\pi r^2) = x/(2r) = x/d$.

Note S5: Consideration of Focusing for Fluorescence Intensity Integration

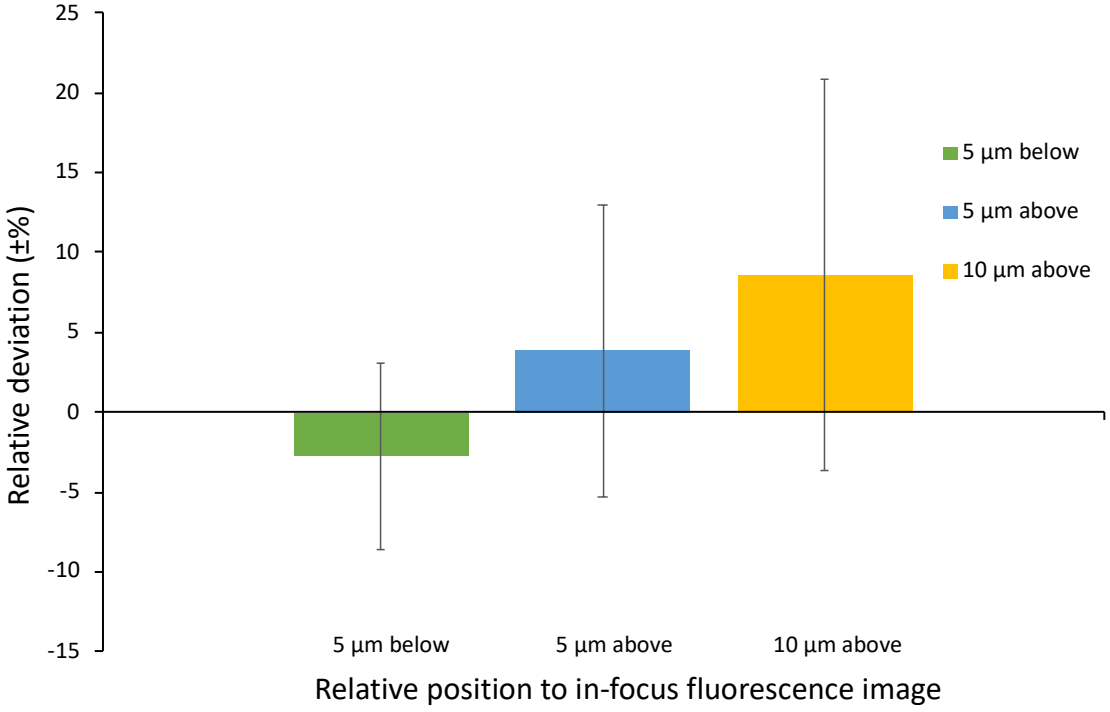

Figure S3. Average relative deviations in fluorescence intensities at different Z positions. Cells were stained with 2 µM cytoplasmic probe DRAQ9. Cell contours were determined from taking an in-focus BF image. An in-focus fluorescence image was taken for reference and fluorescence images 5 µm below, 5 µm above, and 10 µm above the reference were taken. Intracellular fluorescence intensities obtained from the in-focus image were used to find relative deviations in intensities for the out-of-focus images. The average relative deviations were –2.2 ± 5.8%, 3.8 ± 9.1%, and 8.5 ± 12.2% for fluorescence images taken 5 µm below, 5 µm above, and 10 µm above the reference, respectively.

Note S6: Considerations on Statistics

In our case, we were interested to compare the k_{efflux} distributions obtained from the original and new workflow, respectively. To help us choose the most appropriate statistical test, and to guide us for future experiments, we formulated a series of questions:

1) Is the data qualitative (*e.g.*, percentages, frequencies) or quantitative (*e.g.*, mean, median)
2) How many samples are we testing? If you are testing more than one group, are the groups independent or paired?
3) What is the purpose of the test? Here, there are three options: *i)* testing against a hypothesized value, *ii)* compare two (or more) populations, *iii)* establish a correlation.
4) Does the data follow a normal distribution? If yes, then use a parametric test. If not, use a non-parametric test.

We established that:

1) Our data was quantitative (k_{efflux} values)
2) Two independent groups (k_{efflux} values from the original workflow *vs* k_{efflux} values from the new workflow). Usually, two groups are considered dependent if the measurements in one group affect or are somewhat related to the measurements in the other group (*e.g.*, measuring heart pressure from the same individual before and after the administration of hypertension medications). On the other hand, two groups are considered independent if their values do not depend on each other (*e.g.*, measuring heart pressure from a group that was treated with hypertension medications and from another group that was treated with a placebo drug) . In our case, although the measurements were done on the same set of cells, the groups were deemed independent because each workflow computed its own set of measurements independently.
3) The purpose is to test the two distinct k_{efflux} distributions.
4) In our case, a visual representation (Figure 6 main text) was enough to establish that our data was not normal. Sometimes, this is not possible, and an appropriate normality test is required, *e.g.*, the Shapiro-Wilks normality test.

Based on our answers, we established that the two-sample Kolmogorov-Smirnov test was appropriate to conduct our analysis. Essentially, this test estimates the probability that two groups were drawn from the same hypothetical distribution by detecting differences in both the locations (median values) and shapes (skewness values) of the distributions. The test does so by comparing the two empirical distribution functions (EDF). In general, an EDF assigns a specific probability value to every observed event in the group. The largest absolute difference between the two EDFs is referred to as the test statistic for the Kolmogorov-Smirnov test (D):

$$D = |\mathrm{EDF}_{\mathrm{group\ 1}} - \mathrm{EDF}_{\mathrm{group\ 2}}| \qquad (1)$$

where, group 1 and group 2 refer to the two independent groups being compared.

If the D value is greater than the approximate critical value (D_α) for a given α, then the null hypothesis is rejected. The null hypothesis states that the two distributions are drawn from the same probability distribution, while D_α can be calculated using the following formula:

$$D_\alpha = c_\alpha \sqrt{\frac{n_1 + n_2}{n_1 n_2}} \qquad (2)$$

where c_α is a coefficient that depends on α, and n_1 and n_2 are the sample sizes for group 1 and group 2, respectively.

Hence, if we consider our situation, the null hypothesis will state that the k_{efflux} distributions, which were obtained from two different workflows, were drawn from the same hypothetical distribution. If this were true, it would mean that the original and the new workflow process our CRRC data in a nearly identical fashion. We executed the Kolmogorov-Smirnov test using the software OriginPro. In our case, OriginPro computed $D = 0.420$ for $\alpha = 0.001$. $D_\alpha = 0.209$, and it was manually calculated from eq 2 for $c_\alpha = 1.95$, $n_1 = 365$ and $n_2 = 114$. Since $D > D_\alpha$, we concluded that the k_{efflux} distributions were not sampled from the same distribution at the 0.001 significance level. This was also confirmed by a p value of 6×10^{-14} ($p << 0.001$). It is noteworthy that OriginPro computes p values based on Kim and Jenrich (Kim, P. J.; Jenrich, R. I. Tables of exact sampling distribution of the two sample Kolmogorov–Smirnov criterion D_{mn} *(m < n)* Selected Tables in Mathematical Statistics. *American Mathematical Society* **1973,** *1*, 80–129).